Materials Chemistry and Physics 316 (2024) 129126

Contents lists available at ScienceDirect

Materials Chemistry and Physics

journal homepage: www.elsevier.com/locate/matchemphys

Nano-titania and carbon nanotube-filled rubber seed oil as machining fluids

Sunday A. Lawal [a,g], Rasaq O. Medupin [b], Kelvin O. Yoro [c,*], Kingsley O. Ukoba [j], Uzoma G. Okoro [a], Oyewole Adedipe [a], Joseph Abutu [d], Jimoh O. Tijani [e], Ambali S. Abdulkareem [f], Mohammed B. Ndaliman [a], Asipita S. Abdulrahman [h], O. Eterigho-Ikelegbe [i], Tien C. Jen [j]

[a] Department of Mechanical Engineering, Federal University of Technology, Minna, Nigeria
[b] Department of Materials and Metallurgical Engineering, Federal University of Technology, Owerri, Nigeria
[c] Energy Technologies Area, Lawrence Berkeley National Laboratory, 1 Cyclotron Road, Berkeley, CA, 94720, United States
[d] Department of Mechanical Engineering, Taraba State University, Jalingo, Nigeria
[e] Department of Chemistry, Federal University of Technology Minna, Nigeria
[f] Department of Chemical Engineering, Federal University of Technology, Minna, Nigeria
[g] Department of Mechanical Engineering, University of Mines and Technology, Tarkwa, Ghana
[h] Department of Materials and Metallurgical Engineering, Federal University of Technology, Minna, Nigeria
[i] Clean Coal Technology Research Group, School of Chemical and Metallurgical Engineering, Faculty of Engineering and the Built Environment, University of the Witwatersrand, Private Bag X3, Wits, 2050, Johannesburg, South Africa
[j] Department of Mechanical Engineering Science, University of Johannesburg, Auckland Campus, South Africa

HIGHLIGHTS

- Terminalia cattapa leaves are explored for green synthesis of TiO_2 NPs.
- $nTiO_2$-CNTs (7:3 & 5:5) yields RSO-based fluids with superior viscosity & thermal conductivity.
- Well-dispersed $nTiO_2$/CNTs in RSO as $nTiO_2$ CNTs mitigate clustering of CNTs.
- $nTiO_2$/CNT-RSO ratio of 0.5:100 offers highest thermal conductivity of 0.518 W/m°C.
- Textural properties of $nTiO_2$ & mesoporous nature of the nanocomposites favor easy heat transfer.

ARTICLE INFO

Keywords:
Terminalia catappa
Titania
CNTs
Rubber seed oil
Nanofluids

ABSTRACT

Machinists face persistent challenges in managing heat dissipation during cutting operations. To address this issue in an environmentally conscious manner, there is a need for nanofluids crafted from sustainable, eco-friendly materials. This study delves into developing nanocomposites (NCs) of nano-titania ($nTiO_2$) derived from *Terminalia catappa* leaves and carbon nanotubes (CNTs) in varying compositions ($nTiO_2$/CNTs: 90/10, 70/30, and 50/50 wt%). These NCs underwent comprehensive characterization using techniques such as BET, HRSEM/EDX, HRTEM, XRD, and FTIR. The aim was to evaluate their stability as potential fillers in rubber seed oils (RSOs) for machining operations. Furthermore, the homogenous NC samples in RSO revealed distinct polycentric rings, indicating the dispersion of $nTiO_2$ in CNTs, forming Ti–O–C and Ti–O–Ti networks. XRD analysis identified anatase diffraction peaks, though the CNT peaks were less distinct due to overlap with TiO_2 peaks. This successful fusion addresses challenges related to individual fillers, ensuring stable nanosuspension formulation. The TiO_2/CNTs (50/50 wt%) NC emerged as particularly effective in dissipating heat from machining interfaces. The study highlights the nanomaterials' high thermal stability, complementing the abundant unsaturated fatty acids in RSOs to create advanced nanofluids for improved machining. The substantial pore volume and stable nanosuspension formation observed are attributed to the large surface area aiding heat removal. Ultimately, the reinforced RSO with $nTiO_2$/CNTs shows promising potential for safe and efficient machining applications.

* Corresponding author.
E-mail address: kelvin.yoroo@gmail.com (K.O. Yoro).

https://doi.org/10.1016/j.matchemphys.2024.129126
Received 3 November 2023; Received in revised form 20 February 2024; Accepted 22 February 2024
Available online 23 February 2024

1. Introduction

Traditionally, machining operation relies on metalworking fluids (including oils and water) to enhance workpiece surface finishing, prolong tool lifespan, and manage the heat generated by cutting tools. Emulsions combining water and oil have been notably employed as cutting fluids. Metalworking fluid expenditure accounted for around 17% of manufacturing costs, reaching USD 1.1 billion in 2016 and is projected to hit USD 1.5 billion by 2020 [1]. Vegetable oils are fast gaining attention as metal-working fluids [2] and composite reinforced nanofluid is attracting tremendous attention for several machining operations in recent times as it possesses improvement on most demerits of traditional metalworking fluids.

Abbreviation

$nTiO_2$	nano-Titania
CNTs	Carbon nanotubes
NCs	Nanocomposites
NPs	Nanoparticles
TEM	Transmission electron microscopy
SEM	Scanning electron microscopy
BET	Brunuer-Emmett-Teller XRD X-ray Diffractometer
FTIR	Fourier transforms infrared spectroscopy
AA2030	Aluminum alloy 2030
nMQL	Nanofluid minimum quantity lubrication
EDX	Energy dispersive spectroscopy
CVD	Chemical vapor deposition
RSO	Rubber seed oil

Vegetable oils, derived from plants, primarily comprise triglycerides composed of glycerol molecules linked to three fatty acid molecules [3]. The triglyceride structure of vegetable oils provides qualities desirable for an ideal cutting fluid. The long, polar fatty acid chains provide high-strength lubricant films that interact effectively with metallic surfaces; thereby offering frictional and wear resistances [4–6]. Furthermore, the triglyceride structure gives the fluid a high natural viscosity and viscosity index and is responsible for its structural stability over a reasonable operating temperature range. According to Chandrakar and Suhane [7], high flash point and its attendant low vapor pressure and volatility make vegetable oils less hazardous during use coupled with their biodegradability, non-toxicity, and renewability which are essential qualities of a sustainable cutting fluid [8].

Studies have shown that traditional metalworking fluids can cause corrosion with poor lubrication properties [9]. On the other hand, low oxidation stability is one major factor hampering industry acceptance and application of vegetable-based oils as machining fluids [10,11]. In addition, researchers are unanimous in the admittance of the fact that most vegetable oils undergo precipitation, cloudiness, solidification, and poor flow under severe conditions of temperature and pressure [12]. Hence, chemical modifications of the oxidation stability are often undertaken for improvement. It was argued that reducing the level of unsaturated fatty acids, though positive for oxidation stability, could reduce lubrication effectiveness at low temperatures [13]. Therefore, oils containing a large percentage of mono-unsaturated fatty acids are the most likely candidates for machining lubrication. For example, Jatropha oil is said to perform better in terms of power reduction, lubrication, heat dissipation as well and chip disposal against mineral oil emulsion in the milling of AA2030 and AISI 1050 carbon steel [14]. At a much higher temperature, Palm oil was found to be more stable than rapeseed oil and sunflower oil. In another investigation, palm kernel oil, and cottonseed oil were found to perform better than mineral oil in terms of surface roughness, cutting force, and friction reduction during the turning operation of AISI 4340 steel [15]. Oils from groundnut, shear butter, palm kernel, and coconut are also reported to be effective in reducing cutting force/coefficient of friction and improving product quality during cylindrical machining [16]. More recently, corn oil was used by Arsene et al. [17] as a cutting fluid during the hard turning of AIDI D2 hardened steel with ceramic wiper inserts. Findings from their analyses show that a 17.6% reduction in tool wear was achieved when compared to dry machining.

Stakeholders in the food industry have consistently discouraged the use of edible oils as machining fluids even though researchers see many of them as having potential for such applications [18–20]. Rubber seed oil (RSO) is non-edible and eliminates the possible competition with edible oils as a viable alternative. Mohammed et al. [21], Maliki and Ifijen [22], and Ebelewe et al. [23] reported that rubber seed is rich in oil and a relatively cheap source of vegetable oil. Yet is scarcely put to any major economic use. Recently, Osayi et al. [24] found that RSO performs better in terms of surface roughness reduction than mineral oil-based cutting fluid during a turning operation of mild steel. Its performance was also tested against aluminum alloy 6061 using minimum quantity lubrication in a turning operation with a positive report [25].

Despite volumes of reports in favor of different vegetable oils as a lubricating agent during machining, reinforcement with nanoparticles (NPs) has been researched for a better and safer machining experience [26]. Nanosized MoS_2, Al_2O_3, CuO, ZnO, TiO_2, SiO_2, Fe_3O_4, and CeO_2 are being extensively studied as preferred reinforcing agents for nano-cutting fluid production [27–34]. More recently, a combination of more than one NPs is currently receiving greater attention among researchers having successfully exploited the performance of single NP-reinforced base oils for the production of lubricating nanofluids for machining. Amiri et al. [35] reported on the preference of SiO_2–Cu nanocomposite over the nanofluids prepared with only SiO_2 NPs while Toghraie et al. [36] drew a similar conclusion with ZnO–TiO_2 nanocomposite enhanced ethylene glycol hybrid nanofluid. In another investigation, Anand et al. [37] assessed the rheological and machining properties of TiO_2-enhanced rice bran oil in comparison to the performance of TiO_2-graphene nanocomposite improved rice bran oil. Their conclusion was also in the affirmative; favoring the latter. As far as could be ascertained, the formation of NCs with the combination of nanofibres and NPs is scarcely reported in the literature [38]. Particle-particle reinforcement of base oils is more reported in the literature [38–40]. TiO_2 is a nanoparticle while CNT is fibrous in nature and is more thermally stable than TiO_2 [41,42]. Their relationship at the nano level is as important as their reinforcing capability of the vegetable base oil for any application. Therefore, given the critical role nanofillers play in the attainment of sustainable clean machining through the nanofluid minimum quantity lubrication (nMQL) technique, the processes leading to the production of the fillers as well as the nanofluid deserve all the needed attention. On this note, this study is designed to develop and characterize high-quality hybrid nanofluids for machining applications.

In this study, extracts from three plants (*Terminalia catappa, Plumeria acuminate, and Carica papaya leaves*) were selected and quantitatively screened for flavonoids, total phenols, and tannins. Extract of *Terminalia catappa* leaves was found to contain a higher amount of phytoconstituents than the other two and, on this basis, was selected for the green synthesis of TiO_2 nanoparticles. These phytochemical components in plant extracts can perform the same role as expensive commercial and reducing agents such as $NaBH_4$ and $LiAlH_4$ which release toxic chemicals to the environment and compromise environmental safety [42]. Many researchers have leveraged the mechanical strength of hybrid TiO_2-CNTs as reinforcing fillers in natural rubber for structural application with a high rate of success [43,44]. However, their use as additives in RSO as heat-removing enhancers during machining operations has not been adequately reported. This study explores the high thermal stability of the nanomaterials to complement the large concentration of unsaturated fatty acids in RSOs to develop innovative nanofluids for improved machining experience with difficult-to-machine materials.

2. Materials and methods

The first part of this section highlights the underlying theories and mechanisms governing the processes of nanofluid production and application. Subsequently, the various materials and methods used for the synthesis of $nTiO_2$ and CNTs as well as the compounding of the nanofluids are presented in this section. The materials/equipment and their different roles in the study are highlighted in the first part of the section. This is followed by a detailed description of the processes involved in the preparation of the additives and the formulation of the different mass fractions of the hybrid fillers in the rubber seed base oil. This section closes with the characterization methods of the nanomaterials and nanofluids.

2.1. Research theory

The advent and advancement of nanotechnology open many other areas of study to enhance material performance in different fields, nanofluid inclusive. This is achieved by mixing characteristic low-thermal-conductivity base fluid (rubber seed oil in this study), with solid nanomaterials of high thermal conductivity (nano-titania and carbon nanotubes in this case). Ahead of the implementation of nanofluids is the synthesis of the reinforcing fillers. Because of the small size and high surface areas which often lead to agglomeration, the study adopted the two-step method of nanofluid's preparation. As presented in this study, the solid fillers are first synthesized and adequately purified, as well as functionalized to forestall the inherent challenge of clustering before feeding them into the base oil to obtain the nanofluids. This involves ultrasonic agitation, and high shear mixing to homogenize the solid reinforcers in the presence of surfactants to obtain a stable nanosuspension [45].

Following the successful synthesis of nanofillers and the compounding of the nanofluid, cooling, and lubrication mechanisms are other key aspects of this work. The processes come into play at the point of application of the nanofluid where CNTs and $nTiO_2$ nanofillers help to convey heat away from the machining zone and the rubber seed base oil serves as an antifriction agent to ensure that less heat is generated at the interface between the cutting tool and the workpiece during the manufacturing exercise [46]. Detailed theory on the application of nanofluids has been adequately discussed in a recent review by Lawal et al. [26].

2.2. Materials

All reagents used in this study were of analytical grade with percentage purity in the range of 95%–99%. They were sourced from one of the world's most trusted suppliers of high-quality reagents – Sigma Aldrich and used without any further purification. The materials used in this experiment include RSO, *Terminalia catappa* leaves, titanium (IV) isopropoxide (Ti $\{OCH(CH_3)_2\}_4$, methanol (CH_3OH), NaOH pellets, HCl and sodium lauryl sulfate (for regulating the pH of the mixture) as well as distilled water (for washing and purification of the CNTs and TiO_2). Some of the equipment used comprises a 78 HW-1 constant temperature magnetic stirrer for stirring the composites, a high-speed refrigerated centrifuge (model No.LR10-2.4A) for preserving the oils while the experiments last, and Image J software to determine the crystallite size of the spherical-shaped TiO_2 nanoparticles. A UV–visible spectrophotometer (UV-1800) was also employed for evaluating the absorption of ultraviolet light by the nanoparticles while a viscometer (NDJ-5S) was used to measure the viscosity of the nanofluids. Other devices include an electric weighing balance for weight measurement, an ultrasonic oscillator (version KQ3200DB) for higher-level stirring, a muffle furnace for calcination, and chemical vapor deposition (CVD) for the synthesis of CNTs.

2.3. Synthesis of TiO_2 nanoparticles

Green synthesis, based on the use of plant extracts as reducing, capping, and stabilizing agents, is a burgeoning trend compared to other physical and chemical routes used to prepare nanoparticles. Plant materials are relatively available in abundance, cost-effective, and environmentally friendly. TiO_2 nanoparticle synthesis via the green route using an extract of *Terminalia catappa* is a cheaper means as opposed to other synthesis protocols.

20.0 g of freshly chopped *Terminalia catappa* leaves were weighed, washed thoroughly in water placed in a conical flask containing 100 ml of distilled water, and heated on a magnetic stirrer at 60 °C for 20 min to obtain the aqueous leaves extract. It was then filtered into another conical flask giving a yellowish-brown liquid extract. The experiment was carried out according to a design of experiment shown in Table 1, considering four factors: volume of extract, volume of precursor, stirring time, and pH. The Titania nanoparticles extraction process is summarized in Fig. 1.

Conventional optimization of biosynthesis of TiO_2 nanoparticles (where factors are varied while other variables are kept constant) is extremely time-consuming and often amounts to a waste of chemicals. It does not show interrelationships among synthesis parameters. Optimization of synthesis procedure using statistical design of experiment (DOE) involving response surface methodology (RSM) is highly effective and saves time because of a minimum number of experiments based on interactive effects of different process parameters. This interactive effect is expected to guarantee TiO_2 nanoparticles of the desired size and shapes and improved properties. Several parameters influence the shape, size, morphology, optical, and textural properties of TiO_2 nanoparticles among which are the volume of extract, stirring time, volume of precursors, and pH. These synthesis parameters were varied to establish the interactive effects and optimum conditions to synthesize TiO_2 nanoparticles.

For the first run, 80 ml of the aqueous catappa leaf extract was measured and transferred to a clean beaker, after which 8 ml of titanium tetraisopropoxide salt was added and then stirred on a magnetic stirrer at 300 rpm without heating the mixture. The mixture was found to be acidic upon pH check, hence, NaOH was added in droplets until the pH became 7 according to the design. The mixture was placed on the

Table 1
Experimental run for the biosynthesis of TiO_2 NPs.

Run	Vol. of extract (cm^3)	Stirring time (min)	Vol. of precursor(cm^3)	pH	Crystallite size (nm)
1	80	150	8.0	7	–
2	65	150	5.0	12	–
3	65	100	6.5	12	18.92
4	65	150	8.0	2	–
5	65	100	5.0	7	–
6	50	100	6.5	7	10.20
7	65	200	6.5	12	–
8	80	200	6.5	7	–
9	80	150	6.5	12	16.41
10	50	200	6.5	7	–
11	80	100	6.5	7	–
12	80	150	6.5	2	–
13	65	200	6.5	2	8.09
14	50	150	8.0	7	–
15	65	200	8.0	7	11.05
16	65	150	6.5	7	–
17	65	100	8.0	7	9.70
18	50	150	5.0	7	–
19	65	150	5.0	2	7.64
20	65	100	6.5	2	–
21	50	150	6.5	12	14.09
22	80	150	5.0	7	–
23	65	150	8.0	12	–
24	50	150	6.5	2	–
25	65	200	5.0	7	10.15

Fig. 1. Biosynthesis process of TiO_2.

magnetic stirrer and stirred for 150 min, washed severally with distilled water, and allowed to age for about 16 h. Thereafter, dried in an oven at 100 °C for an hour, followed by calcination of the dried sample at 450 °C for 2 h. The product was a white powdered substance indicating the formation of TiO_2 NPs. The same procedure was repeated for other runs according to the DOE in Table 1.

2.4. Synthesis of CNTs

In preparing the catalyst for the synthesis process, 20.2 g of Fe $(NO_3)_3.6H_2O$ and 14.5 g of Ni $(NO_3)_2.6H_2O$ were put in a beaker, after which 50 ml of distilled water was added and stirred to dissolve the metallic salts. Afterward, 10 g of kaolin was added to the resulting dark green solution to obtain a pale green mixture. The mixture thus formed was stirred at 100 rpm for 2 h, after which it was oven-dried at 120 °C. A reddish-brown solid that resulted from the process was crushed in readiness for a good reaction between the carbon source (acetylene gas) and the catalyst during synthesis. The crushed sample was sieved through a 150 μm sieve and calcined at 800 °C for 16 h to completely remove the nitrate contents.

Following successful catalyst synthesis, 1.0 g of the prepared catalyst was spread to form a thin layer in a quartz boat which was then placed in the center of the quartz tube in the CVD machine. Nitrogen, an inert gas, was allowed to flow through the reaction chamber of the CVD at 30 ml/min to ensure an inert atmosphere to avoid any unsolicited reactions. At a reaction temperature of 700 °C, the nitrogen flow rate was adjusted to 100 mL/min. Acetylene gas was introduced into the reaction chamber at 190 ml/min to initiate CNT growth. The flow of acetylene gas was stopped after 90 min and the CVD machine was allowed to cool to room temperature under a continuous flow of nitrogen gas at 30 ml/min. The quartz boat was then withdrawn from the reactor to harvest the CNTs. Each run of the reaction in the CVD machine produced as much as 6.0 g of CNTs. Next, the CNTs were purified using a 3:1 mixture ratio of H_2SO_4 and HNO_3. 15 mL of concentrated HNO_3 was added to a conical flask containing 45 mL of diluted H_2SO_4, after which 10.0 g of the CNTs was introduced into the flask for purification. It was then placed in the ultrasonic cleaner preset to 45 °C and run for 2 h as described by Medupin et al. [47]. After ultra-sonication was complete, the suspension was washed repeatedly in distilled water until a neutral pH was achieved. The CNTs were oven-dried marking the completion of CNTs synthesis.

2.5. Preparation of TiO_2/CNT filled rubber seed oil nanofluid

Nanofluids were prepared with RSO and nanofillers in various concentrations. The nanofillers and their composites used are CNTs, TiO_2, and TiO_2/CNTs (70/30 and 50/50 wt%). Sodium Lauryl Sulfate was used to prevent agglomeration between the NPs. The two-step method of nanofluid preparation as described by Lawal et al. [26] was used in this study. The volume of oil used was kept constant at 100 ml throughout the experiments, while the number of nanofillers was increased from 0.1 g to 0.3 g–0.5 g to also observe the effect of the concentration of the fillers on the base oil. A total of 12 different nanofluids were produced. The design of experiment for this is shown in Table 2.

A 0.1 g of TiO_2 NPs with an equal quantity of sodium lauryl sulfate in 5 ml of distilled water were poured into 100 ml of RSO and then stirred on a magnetic stirrer for 30 min before being ultrasonicated for 40 min.

Table 2
Design of Experiment for preparation of nanofluids.

S/N	Nanofluid prepared	Nanofillers & NCs	Volume of oil (mL)	Filler's quantity (g)
1	Sample 1.1	TiO_2	100	0.1
2	Sample 1.2	TiO_2	100	0.3
3	Sample 1.3	TiO_2	100	0.5
4	Sample 2.1	CNT	100	0.1
5	Sample 2.2	CNT	100	0.3
6	Sample 2.3	CNT	100	0.5
7	Sample 3.1	$nTiO_2$/CNTs (70/30 wt%)	100	0.1
8	Sample 3.2	$nTiO_2$/CNTs (70/30 wt%)	100	0.3
9	Sample 3.3	$nTiO_2$/CNTs (70/30 wt%)	100	0.5
10	Sample 4.1	$nTiO_2$/CNTs (50/50 wt%)	100	0.1
11	Sample 4.2	$nTiO_2$/CNTs (50/50 wt%)	100	0.3
12	Sample 4.3	TiO_2/CNTs (5:5)	100	0.5

During the ultrasonication at a temperature above the boiling point of water, distilled water evaporates from the mixture; leaving behind only dispersed fillers and base oil. Following the Design of Experiment in Table 2, the same procedure was repeated for the remaining nanofluids. The specimens were hereafter characterized.

2.6. Characterization of nanomaterials

The samples prepared in this study were subjected to various characterization techniques. The phase and crystallite sizes of the nanofillers were determined using Bruker AXS D8 Advance X-ray Diffractometer (XRD) with Cu Kα radiation source. The diffractograms were recorded in the 2θ range of 20° to 90° to identify the different phases present.

For the examination of morphology and structure, Zeiss Auriga High-resolution Transmission Electron Microscopy (HRTEM) was employed. To achieve this, 0.02 g of the samples were suspended in 10 cm^3 of methanol and ultrasonicated until complete dispersion was achieved. Nanosuspensions were then placed on a holey carbon grid using a micropipette and dried through exposure to photo light. The morphologies of the nanomaterials were further investigated using Zeiss Auriga High-resolution Scanning Electron Microscopy (HRSEM) with Energy Dispersive Spectroscopy (EDX). A small amount (0.05 mg) of the sample was sprinkled onto carbon adhesive tape and coated with Au–Pd using a Quorum T15OT Analyzer for 5 min. The coated sample was then imaged at high electron tension (5 kV) for analysis. EDX was employed to determine the elemental composition of the materials, operating at EHT for 20 kV.

Additionally, the Brunauer-Emmett-Teller (BET) surface area and pore size distributions of the samples were obtained by analyzing the volume absorbed versus the relative pressure plot. To do this, a predetermined weight of the nanomaterial sample (0.1 g) was placed in a sample tube and degassed at 95 °C for 4 h to remove any residual water and volatile compounds.

2.7. Characterization of nanofluids

A rotational viscometer (model NDJ-8S; serial number N2202 779) was used to carry out all viscosity measurements of the samples in this study. The absolute (dynamic) viscosity measurements of the cutting fluid samples were taken before heating to and at both 40 °C and 100 °C under stirring to determine the viscosity index of each of the cutting fluid samples. The viscosity measurement of RSO was first recorded before those of the nanofluid samples. A thermal conductivity test was carried out using a KHCT-143 machine for liquids. The machine heats a thin layer of liquid and has a cooling plate to remove heat from the liquid layer, ensuring unidirectional heat flow. The input to the heater can be varied and measurement of the input power is done using a digital energy meter and stopwatch. A valve is provided to control water flow. Four temperature sensors also measure temperatures across the liquid layer. The stability of nanofluids was determined using the sedimentation approach. Samples were kept in sample bottles and the time taken for the various NPs to settle down was carefully observed and recorded.

3. Results and discussion

The data gathered after all the experimental procedures as presented in the earlier section and subsections are discussed in this section. The results are first graphically presented before they are logically and scientifically discussed based on theoretical understanding to ensure that the goal of the study is achieved. Furthermore, all the characterization techniques as they relate to individual additive and hybrid nanoparticles and nanofibers are first discussed before their application in heat removal and lubrication during machining operations. The performance characteristics of the additive's concentration in nanofluids are optimized with the optimal combination for kinematic viscosity and thermal conductivity of prepared nanofluids obtained using larger-the-better quality characteristics.

3.1. XRD analysis of optimized CNTs, TiO_2, and TiO_2/CNTs

An experimental design of 2^4 factorials presented in Table 1 was used to investigate the influence of synthesis factors such as stirring time, pH, precursor volume, and extract volume on the yield of the nanofillers. XRD was used to calculate the crystallite size of the analyzed TiO_2. The phase composition was estimated based on the peak intensities of anatase, as presented in Fig. 2. The mean crystallite size was computed from the full width at half maximum (FWHM) of related diffraction anatase peak using the Scherrer Debye equation (Equation (1)). The smallest crystallite size was confirmed at an acidic medium (Table 1). The figures presented as crystallite sizes in Table 1 are average values calculated from the diffraction peaks of the XRD patterns in Fig. 2 using the Scherrer Equation (Equation (1))

$$D = \frac{k\lambda}{\beta \cos\theta} \tag{1}$$

where D is the crystallite size, k is the shape factor (0.94), λ is the wavelength of the X-ray source, and β is the FWHM.

Fig. 3 presents the XRD results of the CNTs, TiO_2, and the composites of TiO_2/CNTs at different compounding ratios prepared by the sol-gel method. The XRD patterns reveal that mainly anatase peaks are found for the TiO_2 at 2 θ = 25.2°, 37.7°, 48°, and 54°. The spectra display the XRD patterns of CNTs, with two peaks observed at around 31.6° and 52.1°. These peaks have been indexed to the reflection of graphite of (002) and (100), respectively. For the TiO_2/CNTs NCs, the diffraction peaks of anatase are identified and the diffraction peaks assigned to CNTs are barely seen (Fig. 3(a)). This could be a result of the overlapping of the main peaks of CNTs with the peaks of TiO_2. It could also be attributed to the high intensity of the diffraction peaks of TiO_2 and the low content of CNTs in the composites. Notably, the width of the XRD peaks at 35.03 and 57.5° was slightly broadened as CNTs were added to the NCs. This process implies that the introduction of CNTs markedly changed the NCs' crystalline size of TiO_2. The 2 θ reflection of anatase in Fig. 3(d and e) disappears owing to the low thermodynamic stability and hence its metastable nature at all temperatures and pressures [48]. The high hole-trapping rate of the materials occasioned by the high probability for the *cis*-coordination polymerization eclipsed the peak seen in the other panels of the XRD patterns in Fig. 3.

3.2. HRSEM of CNTs, TiO_2 and TiO_2/CNTs

Fig. 4 presents high-resolution scanning electron microscopy (HRSEM) images of TiO_2, CNTs, and CNTs/TiO_2 NCs at different ratios. From the image demonstrated in Fig. 4(a), the TiO_2 NPs formed a fleck-like structure. On the other hand, Fig. 4(b) revealed tube-like CNTs with a diameter between 20 and 30 nm and a few agglomerated branches and tiny particles on the surface. The micrographs (Fig. 4(c-e)) demonstrate that TiO_2 NPs are well dispersed on the surface of CNTs. The less identification of CNTs in the NCs was consistent with the CNTs/TiO_2 content ratios in the samples, resulting in a well-homogenized distribution of TiO_2 on the CNTs in TiO_2/CNTs (90/10 wt%) NCs as shown in Fig. 4(c). Comparing the HRSEM images of NCs with the TiO_2 NPs, the presence of

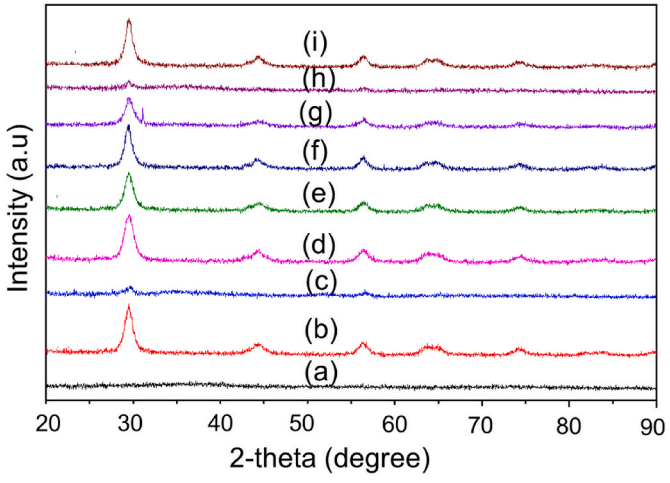

Fig. 2. The XRD patterns of 2^4 factorial design optimizations of biosynthesized TiO_2 NPs for runs (a) 3 (b) 6 (c) 9 (d) 13 (e) 15 (f) 17 (g) 19 (h) 21 (i) 25.

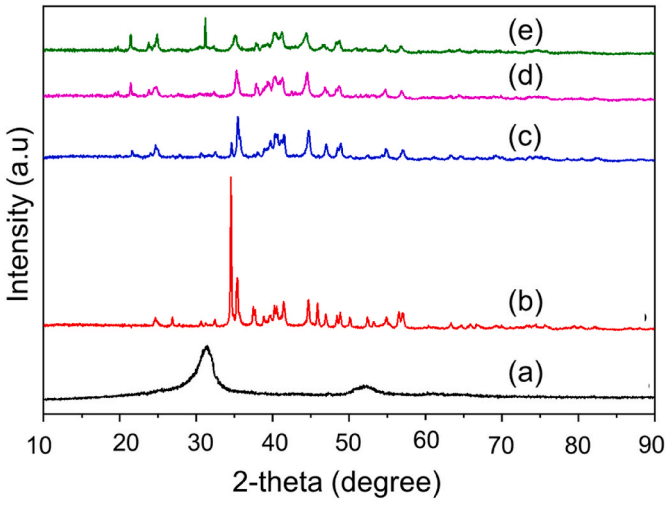

Fig. 3. XRD patterns of (a) CNTs (b) TiO_2 (c) TiO_2/CNTs (9:1) (d) TiO_2/CNTs (7:3) (e) TiO_2/CNTs (5:5).

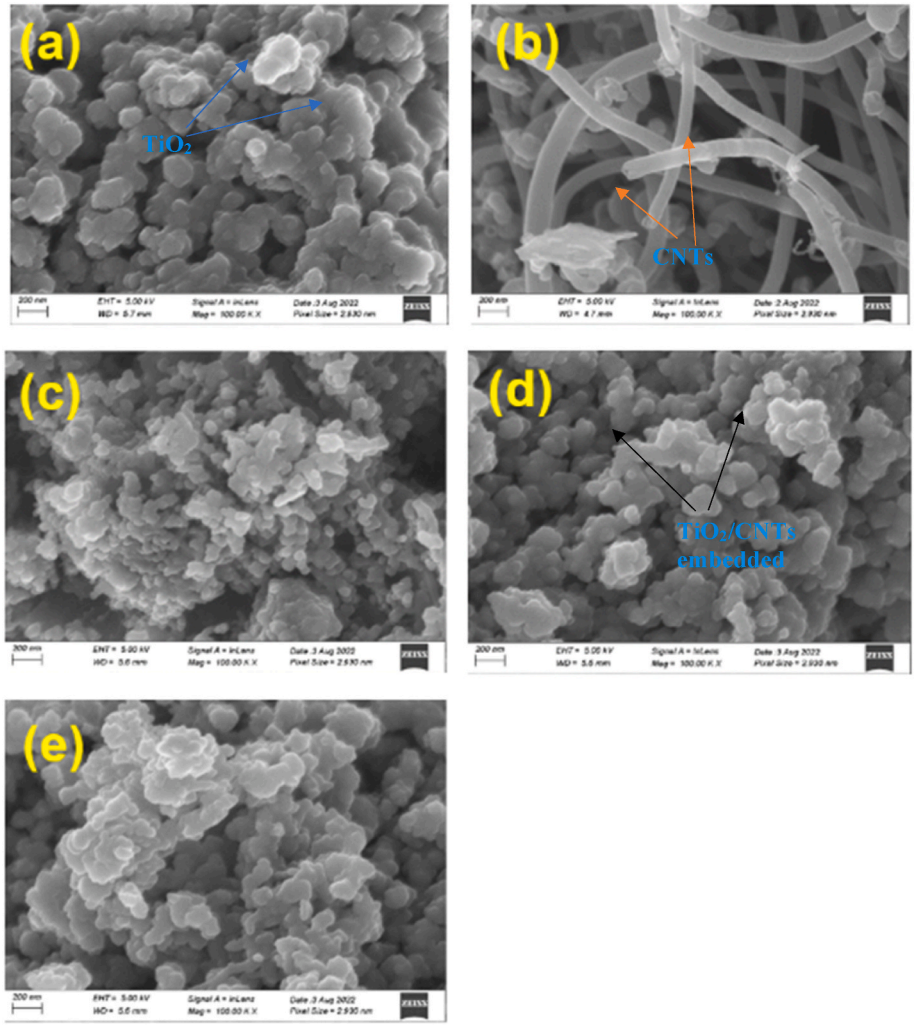

Fig. 4. HRSEM images of (a) TiO_2 (b) CNTs (c) TiO_2 9: CNTs 1 (d) TiO_2 7: CNTs 3 (e) TiO_2 5: CNTs 5.

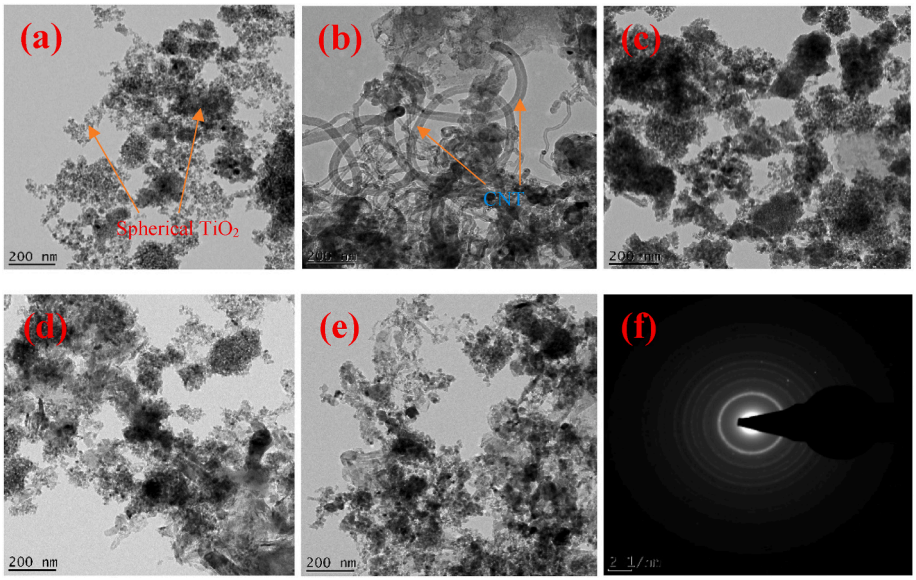

Fig. 5. HRTEM images of (a) $nTiO_2$ (b) CNTs (c) $nTiO_2$/CNTs (90/10 wt%) (d) $nTiO_2$/CNTs (70/30 wt%) (e) nTiO2/CNTs TiO2 (50/50 wt%).

TiO_2 voids or spaces between the particles suggests inter-particle porosity. This suggests that the morphologies obtained for the NCs may be due to the interaction of TiO_2 with the defect sites of the CNTs surface through binding by the intermolecular interaction.

3.3. HRTEM of TiO_2, CNTs and CNTs/TiO_2

Fig. 5 displays high-resolution transmission electron microscopy (HRTEM) images of TiO_2, CNTs, and various CNTs/TiO_2 NCs at different ratios. From Fig. 5(a), spherical TiO_2 NPs are clearly visible while Fig. 5 (b) shows multi-walled carbon nanotubes (MWCNTs) with a hollow structure and varying inner diameters. The HRTEM images of the NCs in

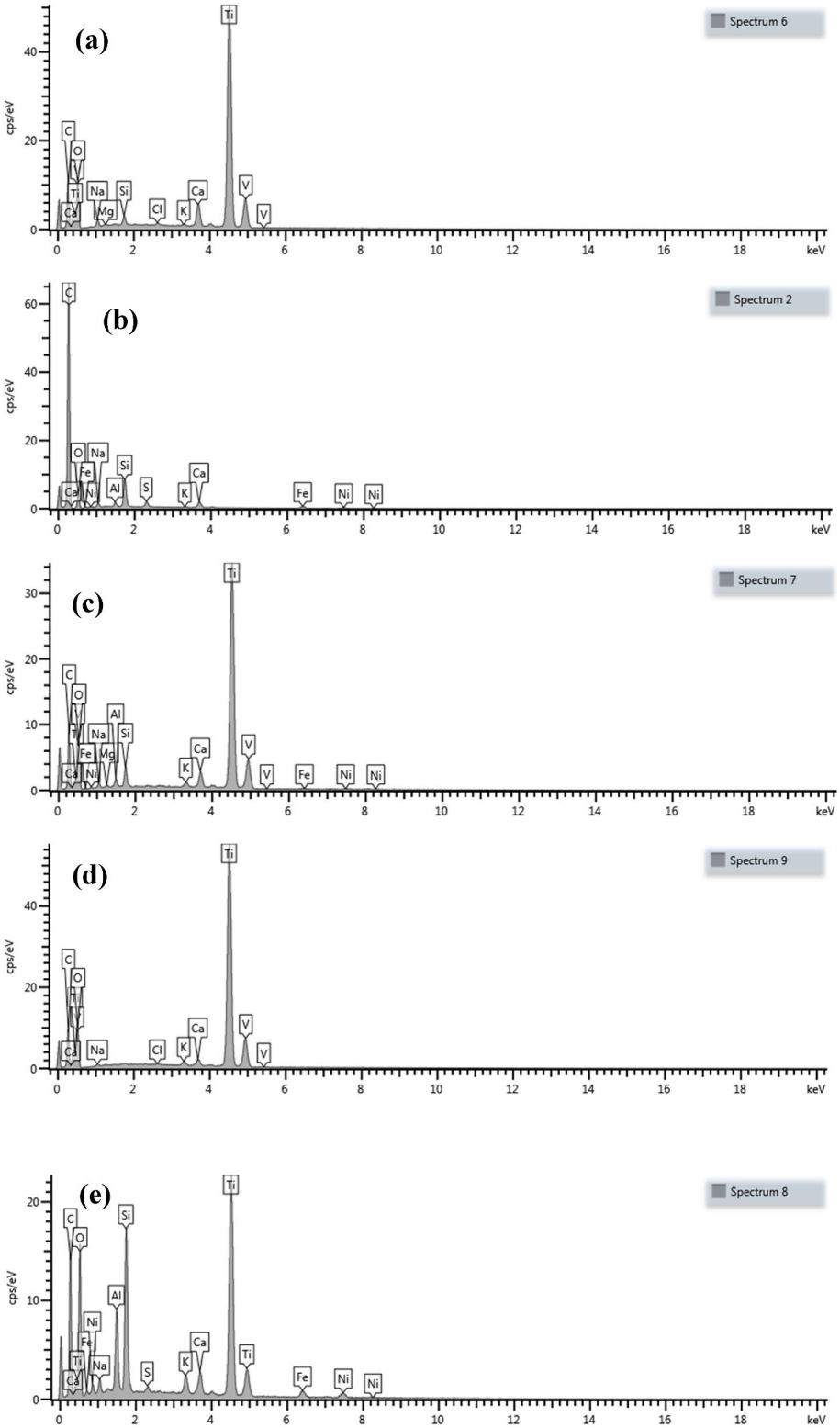

Fig. 6. EDX results of (a) $nTiO_2$ (b) CNTs (c) $nTiO_2$/CNTs (90/10 wt%) (d) $nTiO_2$/CNTs (70/30 wt%) (e) $nTiO_2$/CNTs (50/50 wt%).

Fig. 5(c–e) reveal well-distributed samples where individual CNTs are effectively enclosed within TiO_2, without forming aggregates between TiO_2 and CNTs. The size distribution of TiO_2 measures 14.02 nm, but gradually decreased in the NCs. This phenomenon may be attributed to the interaction between the –OH group on the titania and the chemical groups of CNTs, particularly on the surface defects of acid-pretreated CNTs. These defects may serve as sites of grain growth for TiO_2 crystallites within the NCs.

However, when the CNTs content in CNTs/TiO_2 composites increases, as depicted in Fig. 5(e), the size of the crystallized TiO_2 on the CNTs was reduced, effectively suppressing the agglomeration of TiO_2 NPs. The Selected Area Electron Diffraction (SAED) pattern in Fig. 5(f) reveals characteristic reflections of MWCNTs, while the diffraction pattern for anatase TiO_2 exhibits polycentric rings, as shown in Fig. 6. These findings are consistent with the earlier analysis of XRD. The NCs also exhibit polycentric rings corresponding to different reflection planes, indicating the dispersion of TiO_2 within CNTs to form Ti–O–C and Ti–O–Ti networks.

Furthermore, the energy dispersive x-ray (EDX) spectra in Fig. 6 confirm the presence of Ti, C, and O as the main elements in the NCs, alongside trace elements from the Ni salt and kaolin catalysts. The EDX analysis demonstrates that the Ti content in the NCs follows the mass ratio of the composites.

3.4. BET of TiO_2, CNTs and CNTs/TiO_2

In Fig. 7, the N_2 adsorption-desorption isotherms of CNTs, TiO_2, and CNTs/TiO_2 NCs are depicted (the red curves represents the N_2 adsorption while the black curve represents N_2 desorption), while Table 3 provides the Brunauer-Emmett-Teller (BET) specific surface area, pore

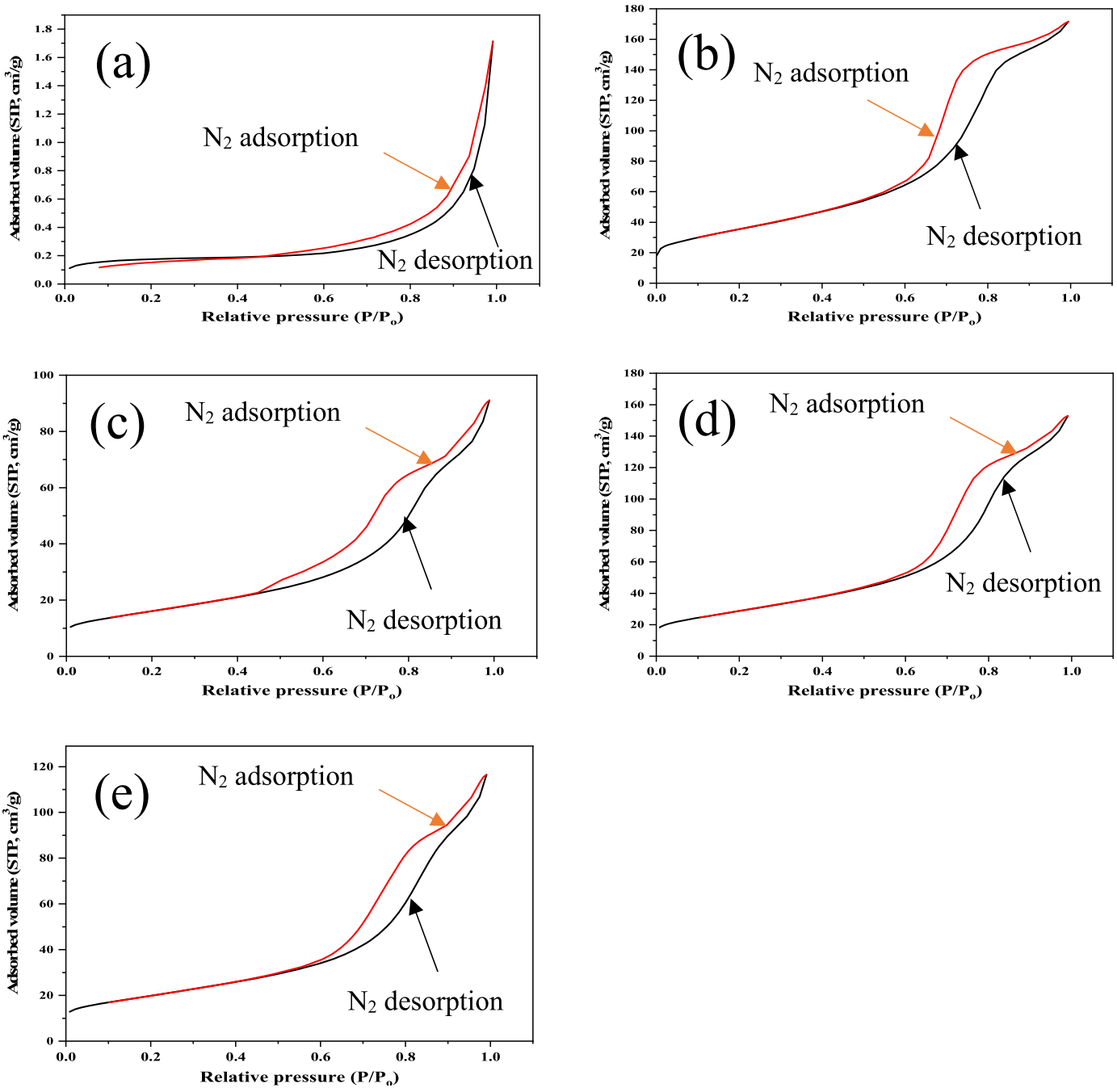

Fig. 7. N_2 Adsorption-desorption curves of (a) CNTs (b) nTiO_2 (c) nTiO_2/CNTs (90/10 wt%) (d) nTiO_2/CNTs (70/30 wt%) (e) nTiO_2/CNTs (50/50 wt%).

Table 3
The summary of BET results of CNTs, TiO_2, and CNTs/TiO_2.

Sample	Surface area (m^2/g)	Pore size (nm)	Pore volume (cc/g)
CNTs	65.00	16.79	0.003
TiO_2	127.62	6.648	0.296
nTiO_2/CNTs (90/10 wt %)	57.84	7.637	0.155
nTiO_2/CNTs (70/30 wt %)	71.19	8.412	0.195
nTiO_2/CNTs (50/50 wt %)	103.42	7.451	0.259

size, and pore volume values for each material. The N_2 adsorption-desorption isotherm of TiO_2 exhibits characteristics consistent with a type IV isotherm, showing a hysteresis loop attributed to capillary condensation. The isotherm identified for the CNTs is the type III isotherm as presented in Fig. 7. The isotherms resulting from the nanocomposite are categorized as type IV isotherms which can be ascribed combination of H2-type and H3-type loops. These isotherms can be explained by introducing the inner cavities of the CNTs. Table 3 presents the BET surface areas of nanomaterials, 65 m^2/g for CNTs, 127.62 m^2/g for TiO_2, 57.84 m^2/g for CNTs/TiO_2 (1:9), 71.19 m^2/g for CNTs/TiO_2 (3:7) and 103.42 m^2/g for CNTs/TiO_2 (50:50 wt%) samples respectively.

The surface area of the as-synthesized nanomaterials was determined using Tristar II 3020 at surface area and pore analyzers based on the N_2 adsorption-desorption method. Thereafter, the surface area determination was carried out by a nitrogen adsorption-desorption isotherm at 77 K, in a Micrometrics ASAP2020 system. Approximately 0.12 g of each synthesized sample was degassed at 95 °C for 4 h to remove any residual impurities blocking the pores.

TiO_2 exhibits a significantly higher surface area than CNTs, indicating superior textural properties and potential for a wide range of applications. Moreover, the surface areas of the NCs show variations with changes in TiO_2 and CNT contents in the samples. This can be attributed to the separation of TiO_2 crystalline particles due to the addition of CNTs. The pore sizes, as presented in Table 3, indicate that the samples are mesoporous nanomaterials, which could facilitate efficient mass transfer. Interestingly, the pore volume of the nanocomposite materials increases as the CNT content increases.

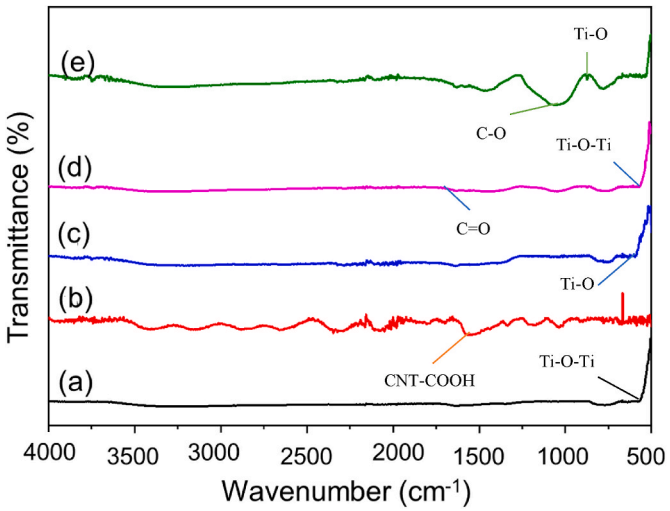

Fig. 8. FTIR spectra of (a) nTiO_2 (b) CNTs (c) nTiO_2/CNTs (90/10 wt%) (d) nTiO_2/CNTs (70/30 wt%) (e) nTiO_2/CNTs (50/50 wt%).

3.5. FTIR of TiO_2, CNTs and TiO_2/CNTs NCs

The Fourier transform infrared spectroscopy (FTIR) was used to investigate the interactions among the different constituents of the NCs and to determine their structure and functional groups. The various FTIR spectra of TiO_2, CNTs, and TiO_2/CNTs are presented in Fig. 8. In Fig. 8 (a), the absorption around 1630 cm^{-1} is attributed to the bending vibration of adsorbed water molecules. The broad band at approximately 950 cm^{-1} in the TiO_2 sample corresponds to the characteristic vibration of the Ti–O–Ti network. For CNTs (Fig. 8(b)), the peaks at 1650 cm^{-1} are assigned to the C–C stretching bonds, representing nanotube modes, while the peak at 1705 cm^{-1} is associated with the C═O stretching of the carboxyl group, indicative of carboxyl functional groups (-COOH). The presence of hydroxyl and carboxyl groups is indicated by the peaks around 3500-3300 cm^{-1}, corresponding to –OH stretching bonds. The FTIR spectra of TiO_2/CNTs (Fig. 8(c, d, and e)) reveal absorption peaks corresponding to C═C and Ti–O bonds, leading to peaks assigned to Ti–O–C and C–O bonds. These results suggest the formation of heterojunction at the surface of the TiO_2 and CNTs, resulting in interfacial bonds in the matrices.

3.6. Viscosity, viscosity index, and thermal conductivity of the nanofluids

3.6.1. Experimental data

Dynamic viscosity was carried out to estimate the amount of resistance offered by each fluid against the action of an external force applied to it. Kinematic viscosity, on the other hand, measures the internal resistance a fluid offers when it is subjected to only gravitational force. The dynamic viscosity results were converted to kinematic viscosity (mm^2/s) using the relationship in Equation (2) with the specific gravity taken to be 0.91 [49]. Table 4 shows the viscosity results for the nanofluid samples at room temperature, 40 °C, and 100 °C.

$$\mu_{kinematic} = \frac{\mu_{dynamic}}{specific\ gravity} \quad (2)$$

Having converted the dynamic viscosities to kinematic viscosities, the viscosity indexes were calculated using an online viscosity index calculator and the results are presented in Table 6. The viscosity of unreinforced RSO as measured by the viscometer was found to be 42.36, equivalent to 46.55 mm^2/s. As seen from Tables 4 and 5, an increase in the filler quantity with the volume of oil kept constant resulted in a corresponding increase in the viscosity of the nanofluids. When 0.1 g of TiO_2 particles was used at room temperature, as in sample 1.1, a viscosity increase of 5.02% was obtained. A percentage increase of 31.82% was obtained when 0.3 g was used (sample 1.2) and 31.6% when 0.5 g was used (sample 1.3). A similar trend was noticed for the CNTs additive. Both dynamic and kinematic viscosity increased as the filler content of the base oil increased from 0.1 g (sample 2.1) to 0.5 g (sample 2.3). This improvement in viscosity can be linked to good dispersion of

Table 4
Design of Experiment for preparation of nanofluids.

S/N	Nanofluids	Dynamic viscosity at room temp. (cp)	Dynamic viscosity at 40 °C (cp)	Dynamic viscosity at 100 °C (cp)
1	Sample 1.1	44.60	38.34	5.54
2	Sample 1.2	55.84	39.69	6.97
3	Sample 1.3	61.93	43.94	7.61
4	Sample 2.1	51.18	39.06	6.72
5	Sample 2.2	60.87	42.51	7.48
6	Sample 2.3	62.04	48.31	11.37
7	Sample 3.1	66.92	46.30	6.21
8	Sample 3.2	70.93	48.25	10.47
9	Sample 3.3	79.85	51.35	11.76
10	Sample 4.1	60.89	45.73	6.11
11	Sample 4.2	65.63	46.24	7.61
12	Sample 4.3	76.35	55.89	12.24

Table 5
Design of Experiment for preparation of nanofluids.

S/N	Nanofluid	Kinematic viscosity at room temperature (mm^2/s)	Kinematic viscosity at 40 °C (mm^2/s)	Kinematic viscosity at 100 °C (mm^2/s)
1	Sample 1.1	49.01	42.13	6.09
2	Sample 1.2	61.63	43.62	7.66
3	Sample 1.3	68.05	48.29	8.36
4	Sample 2.1	56.24	42.92	7.38
5	Sample 2.2	66.89	46.71	8.22
6	Sample 2.3	68.18	53.09	12.49
7	Sample 3.1	73.54	50.88	6.82
8	Sample 3.2	77.95	53.02	11.51
9	Sample 3.3	87.75	56.42	12.92
10	Sample 4.1	66.91	50.25	6.71
11	Sample 4.2	72.12	50.81	8.36
12	Sample 4.3	83.90	61.42	13.45

Table 6
Viscosity index and thermal conductivity values of the nanofluids.

S/N	Nanofluid	Viscosity index values	Thermal conductivity (W/m°C)
1	Sample 1.1	85	0.351
2	Sample 1.2	145	0.381
3	Sample 1.3	152	0.402
4	Sample 2.1	137	0.397
5	Sample 2.2	149	0.413
6	Sample 2.3	242	0.425
7	Sample 3.1	84	0.405
8	Sample 3.2	218	0.439
9	Sample 3.3	237	0.467
10	Sample 4.1	82	0.417
11	Sample 4.2	139	0.465
12	Sample 4.3	227	0.518

the additives in the RSO. This observation would not hold beyond 0.5 g as a further increase in filler content could result in an undesirable agglomeration as reported by Abubakre et al. [44] and, hence, make the nanofluid less viscous and less effective as a heat-removing agent during machining.

For instance, in TiO_2/CNTs (70:30 wt %) NCs the viscosity of the nanofluid improved by 36.7% when 0.1 g of it was utilized (sample 3.1). The best improvement in viscosity was recorded for 0.5 g of the NCs (sample 3.2). The viscosity of TiO_2/CNTs (50:50 wt%) NCs increases significantly when compared with the unfilled and single-additive reinforced base oil. While both nanocomposites outperformed the individual additives, the TiO_2/CNTs (70:30 wt%) performed better because there are more sites on the CNTs to host TiO_2 NPs. As a result, reduced the tendency of agglomeration and hence improved dispersion of the additives in the vegetable oil as well as the stability of the nanofluids.

The thermal conductivity results obtained using the thermal conductivity machine are presented in Table 6. As observed from Table 6, the thermal conductivity of the nanofluid samples increases as the concentration of NPs increases. This trend aligns with the findings of Lawal et al. [26], who reported on the dual functions of heat removal from machining interfaces and lubrication of cutting tools performed by nanofluids to reduce friction during the process. Among the samples, Sample 4.3 exhibited the highest heat conduction away from the cutting zone with a value of 0.518 W/m°C, while Sample 1.1 recorded the slowest heat conduction with a value of 0.351 W/m°C. This can be attributed to the high heat absorption capacity of CNTs and TiO_2, which were present as suspended solids and are known to possess higher thermal conductivities than conventional heat transfer fluids such as vegetable oils [44,50,51].

In summary, the existence of higher interface resistance with the fluid layer is a result of the presence of more surface areas in the nanofillers' existence as single entities and thus capable of conducting heat away from cutting zones faster than when they exist in clusters. Almost all the research findings report a negative correlation between particle sizes/concentrations increase and the viscosity of nanofluids. The majority of these reports are based on nanoparticles and their composites. However, the current study focuses on developing nanofluids from RSO and nanoparticles/nanofibers hybrid composite as fillers.

3.6.2. *Optimal combination*

The optimal combination of kinematic viscosity and thermal conductivity of the prepared nanofluids was obtained using larger-than-better quality characteristics (Equation (3)). The signal-to-noise (S/N) ratio values obtained using Equation (3) are presented in Table 7 while the main effect plots which revealed the optimal combination are shown in Figs. 9 and 10. The S/N ratio measures how the response varies relative to the target values under different conditions. Higher values of the S/N ratios identify the control factor settings that minimize the effect of the noise factor [52]. The values presented in Table 7 indicate that the signal level (response value) for kinematic viscosity is greater than the experimental noise level while that of thermal conductivity showed more influence of experimental noise which slightly tends to affect the response or signal values. However, samples with higher S/N ratios showed better signal quality.

$$\frac{S}{N} = -10\,log\frac{1}{n}\left(\sum_{i=1}^{n}\frac{1}{y_i^2}\right) \tag{3}$$

where n is the number of experimental samples and y represents responses of a given factor level combination.

The main effect plots for viscosity and thermal conductivity presented in Figs. 9 and 10 respectively revealed that the optimum combination of the nanofluid can be achieved using 100 mL volume of oil and 0.5 g filler quantity.

4. Conclusion

This study has successfully synthesized and evaluated the performance of nano-TiO_2 and carbon nanotube (CNT), with the formulated hybrid nanocomposites (NCs) as additives in rubber seed oil (RSO) for machining operations. The NCs show polycentric rings of different reflection planes, which assume the nature of the $nTiO_2$ dispersed in CNTs to form Ti–O–C and Ti–O–Ti networks. It has been confirmed in this study that the thermal conductivity of the nanofluid samples increased as the concentration of NPs increased with filler contents not exceeding 0.5 g. These findings are in agreement with previous reports that nanofluids serve the dual functions of heat removal from machining interfaces and lubrication of cutting tools to reduce friction during the process. The optimal $nTiO_2$/CNT hybrid nanofillers-RSO mixing ratio was Sample 4.3 (TiO_2/CNTs (50/50 wt%)) which exhibited the highest heat conduction away from the cutting zone with a value of 0.518 W/m·°C, while Sample 1.1 manifested the slowest heat conduction with a value of 0.351 W/m°C. This observation is attributed to the high heat absorption capacity of CNTs and $nTiO_2$ existing as suspended solids. Finally, this study has confirmed that nano-Titania and CNT-reinforced RSO have higher thermal conductivities than conventional heat transfer fluids like unreinforced vegetable oils.

Table 7
S/N Ratios for Kinematic viscosity and thermal conductivity of Nanofluid.

Nanofluid prepared	Nanofillers & NCs	Vol. of oil (mL)	Filler's quantity (g)	S/N ratio for kinematic viscosity (room temp.) dB	S/N ratio for kinematic viscosity (40 °C) dB	S/N ratio for kinematic viscosity (100 °C) dB	S/N ratio for thermal conduct. dB
Sample 1.1	TiO_2	100	0.1	33.8057	32.4918	15.6923	−9.0939
Sample 1.2	TiO_2	100	0.3	35.7958	32.7937	17.6846	−8.3815
Sample 1.3	TiO_2	100	0.5	36.6566	33.6771	18.4441	−7.9155
Sample 2.1	CNT	100	0.1	35.0009	32.6532	17.3611	−8.0242
Sample 2.2	CNT	100	0.3	36.5072	33.3882	18.2974	−7.6810
Sample 2.3	CNT	100	0.5	36.6731	34.5003	21.9312	−7.4322
Sample 3.1	$nTiO_2$/CNTs (70/30 wt%)	100	0.1	37.3305	34.1309	16.6757	−7.8509
Sample 3.2	$nTiO_2$/CNTs (70/30 wt%)	100	0.3	37.8363	34.4888	21.2215	−7.1507
Sample 3.3	$nTiO_2$/CNTs (70/30 wt%)	100	0.5	38.8649	35.0287	22.2253	−6.6137
Sample 4.1	$nTiO_2$/CNTs (50/50 wt%)	100	0.1	36.5098	34.0227	16.5345	−7.5973
Sample 4.2	$nTiO_2$/CNTs (50/50 wt%)	100	0.3	37.1611	34.1190	18.4441	−6.6509
Sample 4.3	$nTiO_2$/CNTs (50/50 wt%)	100	0.5	38.4752	35.7662	22.5744	−5.7134

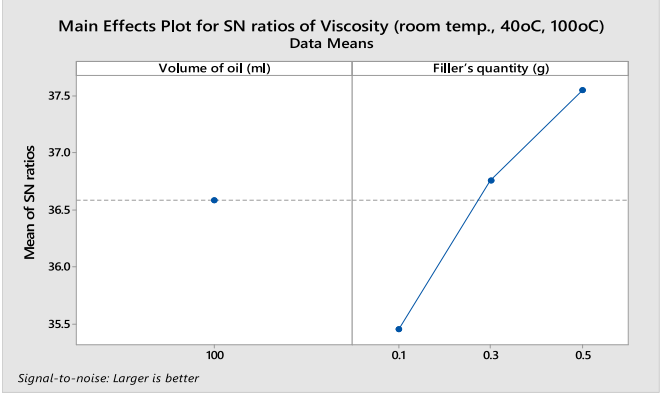

Fig. 9. Optimal parameters for kinematic viscosity of nanofluid.

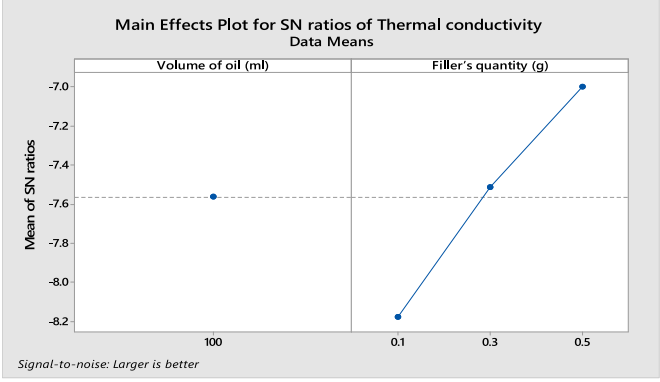

Fig. 10. Optimal parameters for thermal conductivity of nanofluid.

CRediT authorship contribution statement

Sunday A. Lawal: Writing – original draft, Data curation. **Rasaq O. Medupin:** Writing – review & editing, Conceptualization. **Kelvin O. Yoro:** Writing – review & editing, Writing – original draft. **Kingsley O. Ukoba:** Writing – original draft, Formal analysis, Data curation. **Uzoma G. Okoro:** Formal analysis, Data curation. **Oyewole Adedipe:** Methodology. **Joseph Abutu:** Investigation. **Jimoh O. Tijani:** Data curation. **Ambali S. Abdulkareem:** Writing – original draft, Data curation. **Mohammed B. Ndaliman:** Formal analysis, Data curation. **Asipita S. Abdulrahman:** Resources, Methodology. **O. Eterigho-Ikelegbe:** Writing – original draft, Visualization. **Tien C. Jen:** Writing – review & editing, Supervision.

Declaration of competing interest

The authors declare that they have no known competing financial interests or personal relationships that could have appeared to influence the work reported in this paper.

Data availability

Data will be made available on request.

Acknowledgments

The authors gratefully acknowledge the financial support from the National Research Fund (NRF) under the aegis of the Tertiary Education Trust Fund (TETFund), Nigeria, (TETF/ES/DR&D/CE/NRF2020/SETI/113/VOL.1).

References

[1] M.M. Nune, P.K. Chaganti, Development, characterization, and evaluation of novel eco-friendly metal working fluid, Measurement 137 (2019) 401–416. Apr 1.
[2] K.K. Gajrani, M.R. Sankar, Past and current status of eco-friendly vegetable oil-based metal cutting fluids, Mater. Today: Proc. 4 (2) (2017) 3786–3795.
[3] M. Salaheldeen, A.A. Mariod, M.K. Aroua, S.M.A. Rahman, M.E.M. Soudagar, I.M. R. Fattah, Current state and perspectives on transesterification of triglycerides for biodiesel production, Catalysts 11 (2021) 1121, https://doi.org/10.3390/catal11091121.
[4] A. Kumar, A.K. Sharma, J.K. Katiyar, State-of-the-Art in sustainable machining of different materials using nano minimum quality lubrication (NMQL), Lubricants 11 (2023) 64, https://doi.org/10.3390/lubricants11020064.
[5] W. Xu, C. Li, X. Cui, Y. Zhang, M. Yang, T. Gao, M. Liu, X. Wang, Z. Zhou, S. Sharma, Y. Suleiman, Atomization mechanism and machinability evaluation with electrically charged nanolubricant grinding of GH4169, J. Manuf. Process. 106 (September) (2023) 480–493.
[6] X. Zhang, C. Li, Z. Zhou, B. Liu, Y. Zhang, M. Yang, T. Gao, M. Liu, N. Zhang, Z. Said, S. Sharma, H.M. Ali, Vegetable oil - based nanolubricants in machining : from physicochemical properties to application, Chin. J. Mech. Eng. 36 (76) (2023) 3–39, https://doi.org/10.1186/s10033-023-00895-5.
[7] J.K. Chandrakar, A. Suhane, The prospects of vegetable based oils as metal working fluids in manufacturing application –A review, Int. J. Eng. Res. Technol. 3 (5) (2014) 2196–2203.
[8] Y. Singh, A. Yadav, P. Negi, R. Tripathi, Euphorbia lathyris: a novel feedstock for bio-based lubricant application with titanium dioxide nanoparticles as additives, Mater. Today: Proc. 46 (2021) 10518–10522.

[9] N.I. Ncaba, N.E. Wiykiynyuy, T.-C. Jen, K. Ukoba, Effect of thermosyphon limits on design of A taper thermosyphon drill for dry drilling operation, in: IEEE 11th Int. Conf. On Mech. & Intel. Manuf. Technol. (ICMIMT), IEEE, 2020, pp. 118–124, 2020), Jan 20.
[10] G. Gaurav, A. Sharma, G.S. Dangayach, M.L. Meena, Assessment of jojoba as a pure and nano-fluid base oil in minimum quantity lubrication (MQL) hard-turning of Ti–6Al–4V: a step towards sustainable machining, J. Clean. Prod. (2020) 122553, https://doi.org/10.1016/j.jclepro.2020.122553.
[11] R.L. Virdi, S.S. Chatha, H. Singh, Performance evaluation of Inconel 718 under vegetable oils based nanofluids using minimum quantity lubrication grinding, Mater. Today: Proc. 33 (2019) 1538–1545, https://doi.org/10.1016/j.matpr.2020.03.802.
[12] T.P. Jeevan, S.R. Jayaram, Tribological properties and machining performance of vegetable oil based metal working fluids—a review, Mod. Mech. Eng. 8 (2018) 42–65.
[13] Y. Singh, P. Negi, A. Yadav, R. Tripathi, Euphorbia lathyris: a novel feedstock for bio-based lubricant application with titanium dioxide nanoparticles as additives, Mater. Today: Proc. 46 (2021) 10518–10522, https://doi.org/10.1016/j.matpr.2020.12.1237.
[14] R. Amato, C. Wang, R. Calvo, P. Valášek, A. Ruggiero, Characterization of vegetable oil as cutting fluid, Procedia Manuf. 41 (2019) 145–152.
[15] S.A. Lawal, I.A. Choudhury, Y. Nukman, Evaluation of vegetable and mineral oil-in-water emulsion cutting fluids in turning AISI 4340 steel with coated carbide tools, J. Clean. Prod. 66 (2013) 610–618.
[16] S.J. Ojolo, M.O. Amuda, O.Y. Ogunmola, C.U. Ononiwu, Experimental determination of the effect of some straight biological oils on cutting force during cylindrical turning, Revista Mater 13 (4) (2008) 650–663.
[17] B. Arsene, C. Gheorghe, F.A. Sarbu, M. Barbu, L. Cioca, G. Calefariu, MQL-assisted hard turning of AISI D2 steel with corn oil: analysis of surface roughness, tool wear, and manufacturing costs, Metals (2021) 11.
[18] R. Katna, M. Suhaib, N. Agrawal, Performance of non-edible oils as cutting fluids for green manufacturing, Mater. Manuf. Process. (Oct 19) (2022) 1–8.
[19] R.A. Kazeem, D.A. Fadare, O.M. Ikumapayi, S.A. Akinlabi, S.A. Afolalu, E. T. Akinlabi, Analysis of the physicochemical properties of some selected non-edible vegetable oil-based cutting fluids using the design of experiment (DOE) approach, Lubricants 10 (2) (2022) 16. Jan 19.
[20] J.D. Ferwerda, Oil Crops. InCRC Handbook of Tropical Food Crops, CRC Press, 2018, pp. 58–108. Jan 18.
[21] F.U. Mohamme, I.O. Bakare, F.E. Okieimen, Characterization of Rubber Seed Oil Modified for Biolubricant Feedstock Application, TMS 2020 149th Annual Meeting & Exhibition Supplemental Proceedings. The Minerals, Metals & Materials Series, 2020.
[22] M. Maliki, I.H. Ifijen, Extraction and characterization of rubber seed oil, Int. J. Scient. Eng. & Sci. iv (6) (2020) 24–27.
[23] R.O. Ebewele, A.F. Iyayi, F.K. Hymore, Considerations of the extraction process and potential technical applications of Nigerian rubber seed oil, Int. J. Phys. Sci. 6 (2010) 826–831.
[24] A.O. Osayi, S.A. Lawal, M.B. Ndaliman, J.B. Agboola, Performance evaluation of rubber seed oil based cutting fluid in turning mild steel, Nig. J.Technol. XL (4) (2021) 648–659.
[25] P.H. Setyarini, K. Anam, F.H. Prabowo, Evaluation of rubber seed oil as cutting fluid using minimum quantity lubrication in the turning process of AA6061, Int. J. Eng. Trends Technol. LXIX (1) (2021) 198–204.
[26] S.A. Lawal, R.O. Medupin, K.O. Yoro, U.G. Okoro, O. Adedipe, J. Abutu, J.O. Tijani, A.S. Abdulkareem, K. Ukoba, M.B. Ndaliman, P.T. Sekoai, T.-C. Jen, Nanofluids and their application in carbon fiber reinforced plastics: a review of properties, preparation, and usage, Arab. J. Chem. 16 (2023) 104908, https://doi.org/10.1016/j.arabjc.2023.104908.
[27] S. Bhaumik, V. Paleu, S. Sharma, S. Dwivedi, S. Borkar, M. Kamaraj, Nano and micro additivated glycerol as a promising alternative to existing non-biodegradable and skin unfriendly synthetic cutting fluids, J. Clean. Prod. 263 (2020) 121383, https://doi.org/10.1016/j.jclepro.2020.121383.
[28] A.H. Elsheikh, M.A. Elaziz, S.R. Das, T. Muthuramalingam, S.A. Lu, New optimized predictive model based on political optimizer for eco-friendly MQL-turning of AISI 4340 alloy with nano-lubricants, J. Manuf. Process. 67 (May) (2021) 562–578, https://doi.org/10.1016/j.jmapro.2021.05.014.
[29] S. Sakthi, S.R. Hariharan, S. Mahendran, R. Azhagunambi, Effect of nano additives on magnesium alloy during turning operation with minimum quantity lubrication, Mater. Today: Proc. 81 (2) (2021) 787–790, https://doi.org/10.1016/j.matpr.2021.04.238.
[30] S. Dey, N. Moni Reang, M. Deb, P. Kumar Das, Experimental investigation on combustion-performance-emission characteristics of nanoparticles added biodiesel blends and tribological behavior of contaminated lubricant in a diesel engine, Energy Convers. Manag. (2021) 244, https://doi.org/10.1016/j.enconman.2021.114508.
[31] P. Baskaran, R. Saravanan, M. Vignesh, N. Prasanna, C. Gnanavel, D.K. Nagarathi, T. Gopalakrishnan, Influence of molybdenum disulfide particles' concentration on waste cooking oil nanofluid coolant in cutting force reduction on machining SAE 1144 steel, Mater. Today: Proc. (2022) 2–5, https://doi.org/10.1016/j.matpr.2022.02.191.
[32] J. Ni, Z. Cui, C. Wu, J. Sun, J. Zhou, Evaluation of MQL broaching AISI 1045 steel with sesame oil containing nanoparticles under best concentration, J. Clean. Prod. (2021) 320, https://doi.org/10.1016/j.jclepro.2021.128888.
[33] R.O. Medupin, K. Ukoba, K.O. Yoro, T.C. Jen, Sustainable approach for corrosion control in mild steel using plant-based inhibitors: A review, Mater. Today Sustain. 100373 (2023).
[34] H. Sun, T. Ji, H. Bi, M. Xu, L. Cai, M. Manzo, Synergistic effect of carbon nanotubes and wood-derived carbon scaffold on natural rubber-based high-performance thermally conductive composites, Compos. Sci. Technol. (2021) 213, https://doi.org/10.1016/j.compscitech.2021.108963.
[35] M. Amiri, S. Movahedirad, F. Manteghi, Thermal conductivity of water and ethylene glycol nanofluids containing new modified surface SiO_2-Cu nanoparticles: experimental and modeling, Appl. Therm. Eng. 108 (2016) 48–53.
[36] D. Toghraie, V.A. Chaharsoghi, M. Afrand, Measurement of thermal conductivity of ZnO–TiO2/EG hybrid nanofluid, J. Therm. Anal. Calorim. 125 (1) (2016) 527–535.
[37] R. Anand, A. Raina, M.I. Haq, M.J. Mir, O. Gulzar, M. Wani, Synergism of TiO_2 and graphene as nano-additives in bio-based cutting fluid – an experimental investigation, Tribol. Trans. 64 (2) (2020) 350–366, https://doi.org/10.1080/10402004.2020.1842953.
[38] K. Jemielniak, Review of new developments in machining of aerospace materials, J. Machine Eng. 21 (1) (2021) 22–55, https://doi.org/10.36897/jme/132905.
[39] H. Mahmoud, M. Alhajabdalla, M.S. Nasser, I.A. Hussein, R. Ahmed, H. Karami, Settling behavior of fine cuttings in fiber-containing polyanionic fluids for drilling and hole cleaning application, J. Petrol. Sci. Eng. 199 (August 2020) (2021) 108337, https://doi.org/10.1016/j.petrol.2020.108337.
[40] I.P. Okokpujie, L.K. Tartibu, Performance investigation of the effects of nano-additive-lubricants with cutting parameters on material removal rate of al8112 alloy for advanced manufacturing application, Sustainability 13 (15) (2021), https://doi.org/10.3390/su13158406.
[41] P.E. Imoisili, K. Ukoba, T.C. Jen, Physical, mechanical and thermal properties of high-frequency microwave treated plantain (Musa Paradisiaca) fiber/MWCNT hybrid epoxy nanocomposites, J. Mater. Res. Technol. 9 (3) (2020) 4933–4939. May 1.
[42] A.A. Nejhad, B.A. Behbahani, A. Vasiee, M.A. Mehrnia, Identification of phytochemical, antioxidant, anticancer and antimicrobial potential of Calotropis procera leaf aqueous extract, Sci. Rep. 13 (2023) 14716, https://doi.org/10.1038/s41598-023-42086-1.
[43] R.O. Medupin, O.K. Abubakre, A.S. Abdulkareem, R.A. Muriana, A. S. Abdulrahman, Carbon nanotube reinforced natural rubber nanocomposite for anthropomorphic prosthetic foot purpose, Sci. Rep. 9 (1) (2019), https://doi.org/10.1038/s41598-019-56778-0.
[44] O.K. Abubakre, R.O. Medupin, I.B. Akintunde, J.O. Tijani, A.S. Abdulkareem, R. A. Muriana, J.A. James, K.O. Ukoba, T.-C. Jen, K.O. Yoro, Carbon nanotube-reinforced polymer nanocomposites for sustainable biomedical applications: a review, J. Sci.: Adv. Mater. & Dev. 8 (2) (2023) 100557, https://doi.org/10.1016/j.jsamd.2023.100557.
[45] S. Hu, C. Li, Z. Zhou, B. Liu, Y. Zhang, M. Yang, B. Li, Nanoparticle-enhanced coolants in machining: mechanism, application, and prospects, Front. Mech. Eng. 18 (4) (2023) 53, https://doi.org/10.1007/s11465-023-0769-8, 2023.
[46] X. Cui, C. Li, Y. Zhang, W. Ding, Q. An, B. Liu, Comparative assessment of force, temperature, and wheel wear in sustainable grinding aerospace alloy using lubricant, Front. Mech. Eng. 18 (3) (2023) 1–33, https://doi.org/10.1007/s11465-022-0719-x, 2023.
[47] R.O. Medupin, K.O. Ukoba, A.S. Abdulkareem, O.K. Abubakre, T.-C. Jen, Synthesis, and characterization of monometallic cobalt catalyst supported on kaolin for the production of carbon nanotubes, Int. Rev. Mech. Eng. 13 (8) (2019) 454–464, https://doi.org/10.15866/ireme.v13i8.17019.
[48] D.R. Eddy, M.D. Permana, L.K. Sakti, G.A.N. Sheha, S.S. Hidayat, T. Takel, N. Kumada, I. Rahayu, Heterophase polymorph of TiO2 (anatase, rutile, brookite, TiO2 (B)) for efficient photocatalyst: fabrication and activity, Nanomaterials 13 (4) (2023), https://doi.org/10.3390/nano13040704.
[49] S.E. Onoji, A. Igbafe, S.E. Iyuke, Hevea Brasiliensis (Rubber Seed) Oil: Extraction, Characterization, and Kinetics of Thermo-Oxidative Degradation Using Classical Chemical Methods, Energy & Fuels, 2016, pp. 10555–10567.
[50] R.O. Medupin, O.K. Abubakre, A.S. Abdulkareem, R.A. Muriana, S.A. Lawal, Dimensional and thermal reliability of multi-walled carbon nanotube filled natural rubber nanocomposites, Int. J. Eng. Res. Afr. 51 (2020) 177–189.
[51] A. Kaggwa, J.K. Carson, Developments and future insights of using nanofluids for heat transfer enhancements in thermal systems: a review of recent literature, Int. Nano Lett. 9 (4) (2019) 277–288, https://doi.org/10.1007/s40089-019-00281-x.
[52] R.A. Anugraha, M.Y. Wiraditya, M. Iqbal, N.M. Darmawan, Application of Taguchi method for optimization of parameters for improving Soybean cracking process on dry process of tempeh production, IOP Conf. Ser. Mater. Sci. Eng. 528 (2019) 012070.